Available online at www.sciencedirect.com
ScienceDirect
Trans. Nonferrous Met. Soc. China 34(2024) 2987−3001
Transactions of Nonferrous Metals Society of China
www.tnmsc.cn

Acid mine drainage activation mechanism on lime-depressed pyrite flotation from copper sulfide ore

Jia-qiao YUAN[1], Zhan DING[1], Yun-xiao BI[1], Jie LI[1], Shu-ming WEN[1,2,3], Shao-jun BAI[1,2,3]

1. Faculty of Land Resource Engineering, Kunming University of Science and Technology, Kunming 650093, China;
2. State Key Laboratory of Complex Nonferrous Metal Resources Clean Utilization, Kunming University of Science and Technology, Kunming 650093, China;
3. Yunnan Key Laboratory of Green Separation and Enrichment of Strategic Mineral Resources, Kunming University of Science and Technology, Kunming 650093, China

Received 18 February 2023; accepted 20 September 2023

Abstract: The lime-depressed pyrite from Cu differential flotation tailings with acid mine drainage (AMD) as a natural activator was recovered. The effect of AMD on lime-depressed pyrite flotation was investigated by a series of laboratory flotation tests and surface analytical techniques. Flotation test results indicated that AMD could effectively activate the pyrite flotation with a sodium butyl xanthate (SBX) collector, and a high-quality sulfur concentrate was obtained. Pulp ion concentration analysis results indicated that AMD facilitated desorption of Ca^{2+} and adsorption of Cu^{2+} on the depressed-pyrite surface. Adsorption measurements and contact angle analysis results confirmed that adding AMD improved the adsorption amount of SBX collector on the pyrite surface and increased the contact angle by 31°. Results of Raman spectroscopy and X-ray photoelectron spectroscopy analysis indicated that AMD treatment promoted the formation of hydrophobic species (S^0 hydrophobic entity and copper sulfides) and the removal of hydrophilic calcium and iron species on the pyrite surface, which reinforced the adsorption of collector. The findings of the present research provide important theoretical basis and technical support for a cleaner production of copper sulfide ores.

Key words: copper sulfur ore; acid mine drainage; lime-depressed pyrite; flotation; natural activator; activation mechanism

1 Introduction

Copper sulfide ore is one of the most important copper sources for the extraction and production of metal copper [1,2]. Chalcopyrite ($CuFeS_2$) and pyrite (FeS_2) are the typical valuable minerals in copper sulfide ore [3−5]. During the beneficiation of copper sulfide ore, copper−sulfur flotation separation must be conducted to produce a high-quality copper concentrate after the rejection of pyrite [6,7]. Generally, the high-alkali lime process is usually performed at an extremely high pH (pH>11) by adding plenty of lime, and it is widely applied to copper−sulfur flotation separation [8,9]. As a result, chalcopyrite is enriched in the copper concentrate, and the depressed-pyrite enters the tailings. The recovery of lime-depressed pyrite is imperative for the comprehensive utilization of sulfur resources, which is one of the most important materials for the production of sulfuric acid [10,11]. The recovery of pyrite can also prevent the acid mine drainage (AMD) pollution originating from the oxidation of pyrite minerals once exposed to air and water [12,13]. Thus, the beneficiation of lime-

Corresponding author: Shao-jun BAI, Tel: +86-13888400155, E-mail: baishaojun830829@126.com
DOI: 10.1016/S1003-6326(24)66590-8

depressed pyrite provides an easy access to realize profit maximization and cleaner production of copper sulfide ore.

Activators are crucial to reinforcing the flotation of depressed-pyrite with xanthate collectors. Relentless efforts have been exerted on the varieties of activators and the activation mechanism of inhibited pyrite in copper sulfide ores [10,14−16]. Acids and copper ions are frequently cited as the prime examples of such activation [17]. The addition of acids (e.g., $H_2C_2O_4$, H_2SO_4, and H_3PO_4) can remove the hydrophilic calcium and iron species that once wrap on the pyrite surface, resulting in the formation of soluble complexes or insoluble salts, for instance, $CaSO_4$ and $Fe(OH)_3$ in the pulp [14]. After acid and copper ion activation, dixanthogen and Cu-xanthates can form and become responsible for pyrite flotation [18−20]. It follows that the specific hydrophobic/hydrophilic species on the pyrite surface associated with Cu^{2+} activated products warrant further discussion. Notably, most pyrite activation researches have been conducted independently by adding commercial acids and copper ions. The apparent drawbacks of this method include the consumption of large doses of acids and expensive toxic copper sulfate. Hence, the development of cost-effective and environment-friendly technologies to activate inhabited pyrite is a huge interest for the cleaner beneficiation of copper sulfide ore.

AMD forms during the mining and stockpiling of copper sulfide ores after the oxidation dissolution of sulfide minerals [21,22]. AMD is well accepted to be highly acidic (pH =2−4), containing sulfate, iron ions, copper ions, and other non-ferrous metal ions [23−25]. Emissions of AMD are bound to damage ecosystems and human health [26−29]. Therefore, interest in AMD treatment has grown over the past decades. Treatment methods of neutralization, precipitation, oxygen wetland, ion exchange, and permeable reactive barriers have been adopted in real mining sites [26−30]. However, the available treatment methods primarily focus on degrading the contents of H^+, metal, and sulfate ions of the AMD itself, with most of them being unsustainable because of the continuous supply of chemicals, and energy to the affected ecosystem is inevitable. In other words, these available remediation approaches fail to view AMD as a valuable resource. Recently, the AMD activation mechanism on the micro-flotation of pure pyrite which was depressed by a high-alkali solution (HAS) has been studied. AMD has been utilized as a valuable resource instead of traditional activators (such as H_2SO_4 and $CuSO_4$) [31]. AMD is found to remarkably improve the flotation performance of HAS-depressed pyrite, providing an important theoretical basis for the cleaner utilization of AMD in the flotation field. However, the actual application of AMD in the flotation of lime-depressed pyrite ore requires investigation in the future.

In the present study, AMD activation efficiency on lime-depressed pyrite flotation from copper sulfide ore was further investigated through practical and theoretical research. The suitable process and reagent dosage were determined according to the characteristics of the raw ore. The test scheme of one roughing, one scavenging, and three cleanings of lime-depressed pyrite in copper differential flotation tailings was explored by using sodium butyl xanthate (SBX) as the collector and AMD as the natural activator at the laboratory scale. The effect of AMD addition on the improvement in S grade and recovery was systematically examined under various reagent dosages. Emphases were made on the activation mechanism of AMD, as well as on the analysis of specific hydrophobic/hydrophilic species on the pyrite surface based on the flotation tests, contact angle determinations, adsorption test, ion concentration measurements, Raman spectroscopy, and X-ray photoelectron spectroscopy (XPS). The findings of the present study further enriched the flotation theory of pyrite and provided strong technical support for the cleaner production of similar copper sulfide ore.

2 Experimental

2.1 Materials and reagents

Test works were carried out with a sample of ore from a copper sulfide ore obtained from Yunnan Province, China. The main compositions of the ore were analyzed by Kunming Metallurgical Research Institute, China, and the results are presented in Table 1. Based on the chemical analysis, the main compositions of the ore were 0.38% Cu, 8.92% S, 12.87% Fe, 7.64% Al_2O_3 and 61.19% SiO_2. The principal mineral components in the raw ore

samples were determined by powder X-ray diffraction (XRD) analysis (as depicted in Fig. 1). The main sulfide minerals were chalcopyrite ($CuFeS_2$) and pyrite (FeS_2), whereas the main gangue mineral was quartz. Thus, the ore was a low-grade single copper sulfide ore, and the effective recovery of chalcopyrite and pyrite was the key to the beneficiation of this ore.

Table 1 Chemical analysis results of ore samples (wt.%)

Cu	Fe	S	Pb	Zn	Au	Ag
0.38	12.87	8.92	0.0064	0.26	0.20*	<5.0*
SiO_2	MgO	Al_2O_3	CaO	Na_2O	K_2O	
61.19	3.68	7.64	0.60	0.13	0.95	

* g/t

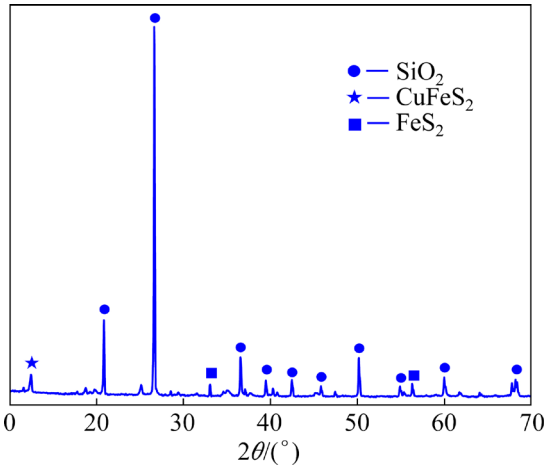

Fig. 1 XRD analysis results for raw ores

The pure pyrite samples for theoretical research (adsorption measurements, contact angle determination, Raman spectroscopy, and XPS) were provided by Yunbaozhai, Yunnan Province, China. Chemical analysis and XRD results showed that the purity of pyrite was 97.5%. AMD was obtained from the Dapingzhang Copper Sulfide Mine of Yunnan Province, China. The AMD used in the flotation study was taken from the wastewater collection pond of the tailing deposit of this copper sulfide mine, which mainly originated from the underground cave mining wastewater and open storage of wastewater in the ore. To avoid variations in AMD composition as much as possible, the sample was stored in an airtight high-density polyethylene container and transported to the laboratory where it was stored at 4 °C until analysis.

The major chemical constituents of AMD were analyzed by inductively coupled plasma (ICP) analysis (ICPS−1000II, Shimadzu, Japan), as displayed in Table 2. The concentrations of Cu^{2+} and SO_4^{2-} in the AMD were 22.8 and 5902 mg/L, respectively, and the pH of AMD was 3.88. The concentrations of Al^{3+} and Mg^{2+} reached 141 and 156 mg/L, which may play a negative role in pyrite flotation [10]. This chemical property of AMD, i.e., being strongly acidic and rich in copper ions, renders it a promising natural activator of lime-depressed pyrite in copper sulfide ores.

The chemical reagents used in this study included pH-adjusting agents, depressors, activators, collectors, and frothers. The details of the reagents adopted in the flotation tests are listed in Table 3. Deionized water with a resistivity of 18 MΩ·cm was obtained from a Milli-Q5O system (Billerica, MA, USA) and was used in all the experiments.

Table 2 Chemical analysis results of AMD

Concentration/(mg·L^{-1})								pH
Cu^{2+}	Pb^{2+}	Zn^{2+}	Fe^{3+}/Fe^{2+}	Al^{3+}	Mg^{2+}	Ca^{2+}	SO_4^{2-}	
22.8	<0.07	30.7	<0.03	<0.03	141	156	5.12	5902	3.88

Table 3 Reagents used in flotation tests

Reagent	Purity	Function
Lime	Analytical grade (>98%)	Pyrite depressant
H_2SO_4	Analytical grade (>98%)	Activator
$CuSO_4$	Analytical grade (>98%)	Activator
$H_2C_2O_4$	Analytical grade (>99.5%)	Activator
NH_4HCO_3	Analytical grade (>98%)	Activator
$FeSO_4$	Analytical grade (>98%)	Activator
Acid mine drainage	–	pH-adjusting agent and activator
Sodium butyl xanthate	Analytical grade (>98%)	Pyrite collector
Potassium ethyl xanthate	Analytical grade (>95%)	Chalcopyrite collector
Terpenic oil	Analytical grade (>95%)	Frother

2.2 Flotation tests

An XFD flotation equipment (Jilin Exploring Machinery Plant, China) was adopted for the flotation tests. Cu differential flotation with high-alkali lime process (pH 11.3), as depicted in Fig. 2, was applied to the beneficiation of copper sulfide ore on the basis of on-spot craft. Lime (5 kg/t), potassium ethyl xanthate (PEX) (60 g/t) and pine oil (30 g/t) were sequentially added into the flotation cell for the collecting of chalcopyrite. The Cu rougher concentrate was acquired after 4 min of flotation.

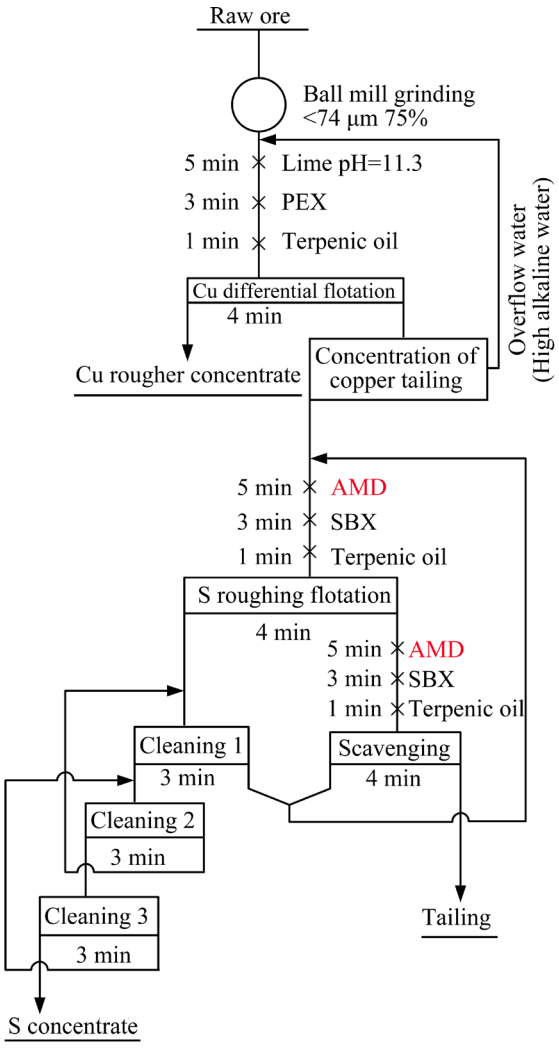

Fig. 2 Flow sheet of closed-circuit flotation of copper sulfide ore with AMD as activator

Flow sheet consisting of one roughing, one scavenging, and three cleanings was conducted to recover pyrite from the tailings of Cu differential flotation. Different types of activators were added to the roughing and scavenging processes. Meanwhile, SBX was used as the collector. The AMD activation effects on lime-depressed pyrite flotation were investigated with emphasis. Each experiment was carried out three times to obtain the mass balance, and flotation efficiency was evaluated by calculating the recovery of S and Cu.

2.3 Ion concentration measurements in flotation pulp

The flotation pulps obtained with different dosages of AMD were extracted into a centrifuge tube, and then placed in a centrifuge (TL−4.7W, SCI, China) under stirring at 3500 r/min for 15 min. The concentrations of Cu^{2+} and Ca^{2+} in the supernatant were determined by ICP analysis. Each experiment was carried out three times to obtain the average value as the final result. To reflect the variation in target ion concentrations in the pulp, the theoretical ion concentrations (Ca^{2+} and Cu^{2+}) were calculated, which included ion concentrations in the pulp and the corresponding ion concentrations in the AMD.

2.4 Adsorption measurements and contact angle determination

Collector adsorption measurements were carried out on a UV−Vis spectrophotometer (UV765, Shanghai, China). The adsorption amounts of SBX on the pyrite surface in the following two systems were investigated: (1) lime-depressed pyrite, i.e. 2 g of pure pyrite was mixed with 40 mL of deionized water, and lime was added to adjust the pH to 11.3 for 15 min; (2) AMD-activated pyrite, i.e., the pyrite sample was treated according to the first system procedure, and then 1.8 m^3/t AMD was added to the solution to react for 15 min. Next, SBX (1.5×10^{-4} mol/L) was added to the two systems, respectively, and adjusted for 60 min at 1700 r/min to ensure equilibrium in the adsorption process. Finally, the suspension was centrifuged and the supernatant was taken to measure the residual SBX concentration. Each condition was repeated three times to obtain the mean value as the final result, and the standard deviation was indicated by error bars. The adsorption amount of SBX on the pyrite surface was calculated according to the following equation:

$$\Gamma=\frac{(C_0-C_t)}{m}V \quad (1)$$

where Γ is the adsorption amount of SBX (mol/g); C_0 and C_t are the initial and residual concentrations of SBX (mol/L), respectively; V is the supernatant fluid volume (L); m is sample mass (g).

Pyrite samples were polished with 2000, 4000, and 6000 grit Al_2O_3 sandpaper to ensure a sufficiently smooth surface. The polished samples were washed with deionized water, then placed in a beaker containing 40 mL of deionized water, and treated with lime, lime-AMD, and SBX collector sequentially according to the same procedure described in adsorption measurements. The treated samples were performed using a contact angle analyzer (JY−82, China). For each experiment, a drop of deionized water was placed into the sample surface through a syringe. The shape of the drop was measured after the three-phase contact angle stably formed. Each experiment was carried out three times, and the average value was taken as the final result.

2.5 Raman spectroscopy measurements

Raman spectra were obtained on a Raman spectrometer (LabRAM HR Evolution HORIBA, France). The Raman spectral resolution varied between 0 and 1000 cm^{-1} with a step width of 1 cm^{-1}. Two samples, i.e., lime-depressed pyrite and AMD-activated pyrite were prepared according to the same procedure above-mentioned in Section 2.4. The Raman spectrum of the original chalcopyrite sample was served as a control. Before each experiment, the spectrometer was calibrated to the vibrational Raman band of silicon at approximately 520 cm^{-1}. Spectral operations such as baseline adjustment, smoothing, and normalization were performed by using Labspec 4.02 software.

2.6 XPS measurements

XPS spectra were obtained using a Versa Probe II X-ray photoelectron spectrometer (PHI 5000, ULVAC-PHI, Japan) equipped with an Al K_α X-ray source under ultrahigh vacuum conditions. 2 g of pure pyrite sample was mixed with 40 mL of deionized water. After adjusting the pH to 11.3 by adding lime and stirring for 15 min, AMD was added subsequently and stirred for 15 min, whereas no AMD was added into the other beaker for contrast testing. The sample was removed by filtration, repeatedly rinsed with the corresponding solution, and dried in a vacuum drying oven (DZF−6021, Shanghai Yiheng Scientific Instrument Co., Ltd.) at 25 °C. A survey scan of the analyzed sample was first conducted to detect elemental compositions and binding energies. Then, peak fitting was performed to investigate the high-resolution scan data.

3 Results and discussion

3.1 Flotation behavior

3.1.1 Effects of different activators on flotation of pyrite

To investigate the activation effect of different activators on lime-inhibited pyrite, H_2SO_4, $H_2C_2O_4$, NH_4HCO_3, $FeSO_4$, H_2SO_4−$CuSO_4$, and AMD were selected as its activators. The specific flotation conditions were as follows: particle size distribution below 74 μm accounted for 75%, and SBX dosage was 100 g/t. Results of flotation tests with different optimum activator dosages are listed in Table 4.

From the comparison results in Table 4, it is clear that the lime-depressed pyrite was basically not recovered without adding any activator. The fact that different types of activators were added under the same agent regime and process flow showed that different flotation indexes were obtained. In a comprehensive comparison, NH_4HCO_3 and $H_2C_2O_4$ exerted a more obvious activation effect on the lime-inhibited pyrite compared with no activator. $FeSO_4$ was beneficial to improving the S grade in a weak alkaline environment, whereas the full activation of lime-depressed pyrite was difficult by using single H_2SO_4. At the sulfuric acid dosage of 5000 g/t, pyrite recovery was increased by approximately 6% after adding 100 g/t of $CuSO_4$ compared with the single use of H_2SO_4. The activation performance of AMD was comparable to that of H_2SO_4−$CuSO_4$, and their activation effects were more effective than those of several other activators. Thus, the effect of AMD on the activation of lime-depressed pyrite will be analyzed with emphasis as follows.

3.1.2 Effects of AMD dosage on pyrite flotation

Based on the unique acidity and high Cu^{2+} concentration of AMD, AMD activation of pyrite in Cu differential flotation tailings was investigated. The results are presented in Fig. 3(a). The specific flotation conditions were as follows: particle size distribution below 74 μm accounted for 75%, and SBX dosage was 100 g/t.

Table 4 Different activator types of pyrite and comparative test results

Activator	Dosage/(g·t^{-1})	pH value of pulp	S grade/%	S recovery/%
No activator	0	11.3	53.18	8.75
H_2SO_4	5000	6.8	50.91	72.29
$H_2C_2O_4$	2000	8.5	51.50	72.41
NH_4HCO_3	3000	8.6	51.64	73.20
$FeSO_4$	3500	8.4	52.89	76.03
H_2SO_4+$CuSO_4$	5000+100	6.9	52.61	78.36
AMD	1.8*	8.5	52.47	80.09

* m^3/t

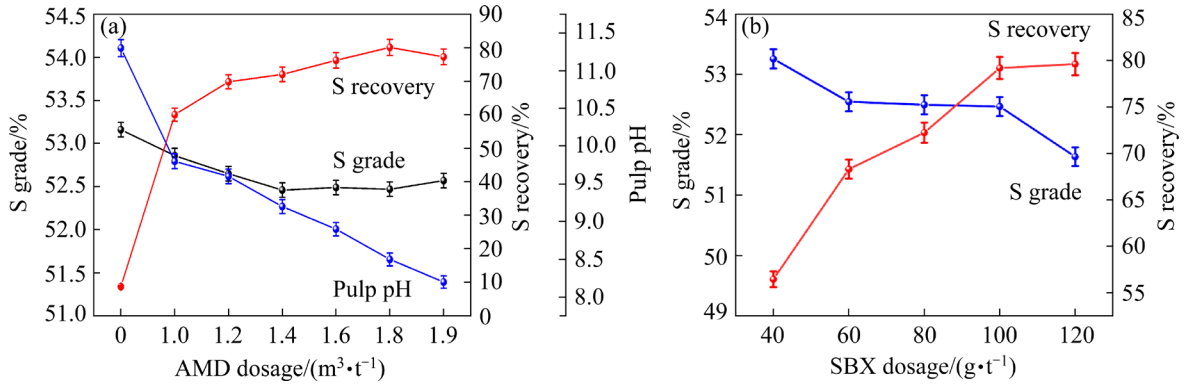

Fig. 3 Effects of AMD (a) and SBX (b) dosages on pyrite flotation

As depicted in Fig. 3(a), AMD played a positive role in pH adjustment and S recovery. The pulp pH was 11.3, and the S recovery was only 8.75% in the absence of AMD, indicating that pyrite was subjected to serious inhibition by lime. With increased AMD dosage, the pulp pH decreased considerably. Obviously, the remarkable decrease in the pulp pH caused by AMD created favorable conditions for the flotation of lime-depressed pyrite. The maximum S recovery of 80.09% was obtained at 1.8 m^3/t AMD dosage, which increased by about 70% compared with the corresponding result in the absence of AMD. In addition, the influences of SBX dosage on the recovery and grade of S are shown in Fig. 3(b) (conditions: AMD dosage of 1.8 m^3/t and rougher pulp pH of 8.5). It is proved that the recommended SBX dosage was 100 g/t, and the corresponding S grade and recovery were 52.47% and 79.22%, respectively. These results confirmed that AMD can effectively activate the flotation of lime-depressed pyrite. It is possible that AMD may have effectively removed the hydrophilic species (Ca^{2+}, $CaOH^+$, and FeOOH) once wrapped on the pyrite surface after the acid−base neutralization reaction. Meanwhile, the adsorption of Cu^{2+} stemming from the AMD can increase the Cu-active sites on the pyrite surfaces, which benefited the adsorption of the collector onto mineral surfaces. Notably, the changes in the S grade of the concentrates were inconspicuous, indicating that the inclusions of gangue minerals were negligible during AMD activation pyrite flotation processing. Thus, AMD dosage was determined to be 1.8 m^3/t in the sulfur rougher stage, and the rougher pulp pH was 8.5. Given these results, adding AMD facilitated the flotation of lime-depressed pyrite, and it can be viewed as a promising natural activator. This activity provided an innovative path to the comprehensive utilization of AMD, with vital practical significance for the emission reduction of AMD and increased beneficiation profits.

3.1.3 Locked-cycle flotation test results of copper sulfide ore

The locked-cycle flotation tests of copper sulfide ore were carried out according to the optimum conditions acquired in the open-circuit flotation experiments, as depicted in Fig. 2. The

experiment results are illustrated in Table 5. As can be seen from Table 5, the recoveries of S and Fe in the sulfur concentrate were 79.82% and 48.69%, with grades of 51.16% and 42.54%, respectively, in the H_2SO_4−$CuSO_4$ system. When AMD (1.8 m^3/t) was used as an activator, the recovery of S was 82.95% with a grade of 51.08%. This concentrate product was a high-quality sulfur concentrate and can meet the needs of sulfuric acid production desirably. The recovery of S in the AMD system was improved by 5.33% compared with the former S flotation index. Thus, the locked-cycle flotation tests of copper sulfide ore provided strong evidence that AMD can effectively activate the pyrite flotation once depressed by lime in copper sulfide ore separation. This method provided a novel approach to AMD treatment, and formed an innovative flotation technology consisting of Cu differential flotation with high-alkali lime and pyrite recovery with AMD activation. Obviously, the application of AMD in copper sulfide flotation had considerable economic and environmental benefits. This work can economize the great mass of fresh water, and AMD may be viewed as a promising natural activator instead of traditional chemical reagents (such as H_2SO_4 and $CuSO_4$), thereby increasing the economic benefits to the flotation plant. Moreover, it can provide easy access to the comprehensive utilization of AMD, exhibiting vital practical significance for the emission reduction of AMD.

3.1.4 Ion concentration in flotation pulp

To explore the effect of AMD on the ion concentration in flotation pulp and indirectly analyze its activation mechanism on the lime-depressed pyrite, the Ca^{2+} and Cu^{2+} concentrations in the pulp were analyzed, as presented in Figs. 4(a) and (b). Figure 4(a) showed that the theoretical concentration of Ca^{2+} increased linearly with increasing AMD dosage. The Ca^{2+} concentration in the pulp (sulfur rougher) without AMD addition was 587.8 mg/L, whereas the Ca^{2+} concentration

Table 5 Locked-cycle flotation tests results of copper sulfide ores

Condition	Product	Yield/%	Grade/%		Recovery/%	
			S	Fe	S	Fe
AMD system	Copper rougher concentrate	5.75	18.47	25.66	11.81	11.68
	Sulfur concentrate	14.60	51.08	43.55	82.95	50.34
	Tailing	79.65	0.36	6.02	5.24	37.98
	Feed	100.00	8.99	12.63	100.00	100.00
H_2SO_4−$CuSO_4$ system	Copper rougher concentrate	6.09	20.23	26.09	13.41	12.68
	Sulfur concentrate	14.34	51.16	42.54	79.82	48.69
	Tailing	79.57	0.86	6.12	6.77	38.63
	Feed	100.00	9.19	12.53	100.00	100.00

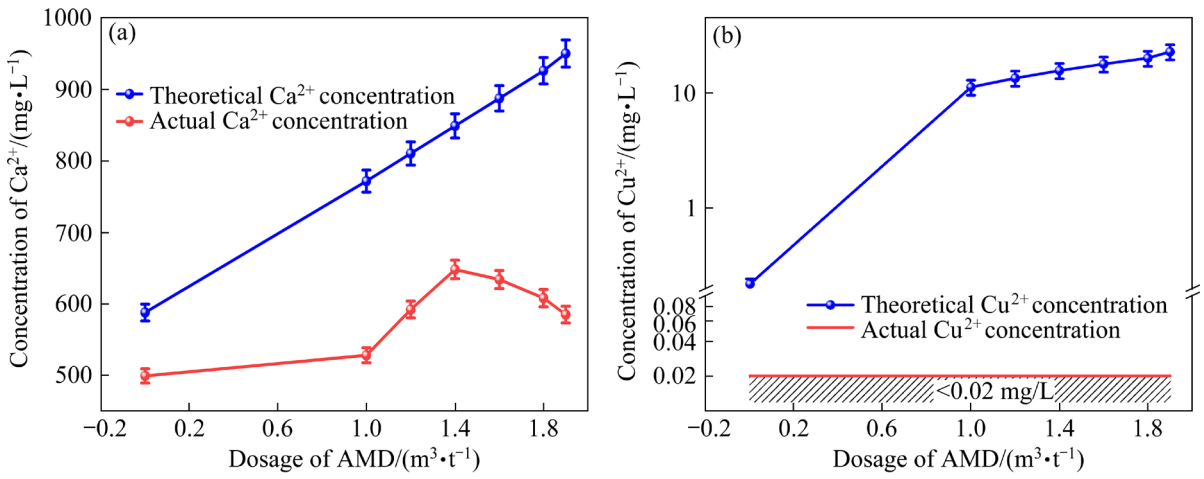

Fig. 4 Variation of Ca^{2+} (a) and Cu^{2+} (b) concentrations in pulp with different AMD dosages

decreased to 499 mg/L after the pre-removal of high alkaline water. This result indicated that the desorption of numerous Ca^{2+} located on the pyrite surface occurred. The actual Ca^{2+} concentration increased remarkably with increasing AMD dosage ranging from 0 to 1.4 m^3/t, and then gradually decreased with further increasing AMD dosage. Notably, the actual Ca^{2+} concentration was significantly smaller than the theoretical concentration of Ca^{2+}. These results indicated that the spontaneous reactions between Ca^{2+} and SO_4^{2-} stemming from AMD occurred and promoted the formation of calcium sulfate precipitate ($CaSO_4{\cdot}2H_2O$). This phenomenon facilitated the desorption of Ca^{2+} located on the lime-depressed pyrite surface, thereby increasing the hydrophobicity of minerals. From Fig. 4(b), the theoretical concentration of Cu^{2+} in the initial pulp was 0.22 mg/L, and it increased with increasing AMD dosage. However, actual Cu^{2+} concentration was all below 0.02 mg/L, which was the lower limit of detection. This finding suggested that Cu^{2+} originating from the AMD can be adsorbed onto the pyrite surface completely, improving the Cu active sites on the lime-depressed pyrite surface. Given these results, adding AMD provided favorable conditions for the flotation of lime-depressed pyrite. The desorption of Ca^{2+} and the increase of Cu-active sites on mineral surfaces played an essential role in pyrite activation.

3.2 Flotation mechanisms

3.2.1 Adsorption and contact angle

Adsorption analysis and contact angle determination were conducted to investigate the effect of SBX collector on the hydrophobicity of lime-depressed pyrite in the presence and absence of AMD. As depicted in Fig. 5, the contact angle of lime-depressed pyrite after the adsorption of SBX collector in the absence of AMD was about 40°, which was much lower than that of natural pyrite once it interacted with xanthate (87.5°) in deionized water, as reported by YANG et al [32]. Meanwhile, the adsorption amount of SBX on the lime-depressed pyrite surface was only 0.018×10^{-5} mol/g. These results confirmed that pyrite was subjected to serious inhibition by lime and failed to adsorb the SBX collector. The contact angle of AMD-activated pyrite increased to 71°, and the adsorption amount of the SBX collector reached 0.053×10^{-5} mol/g,

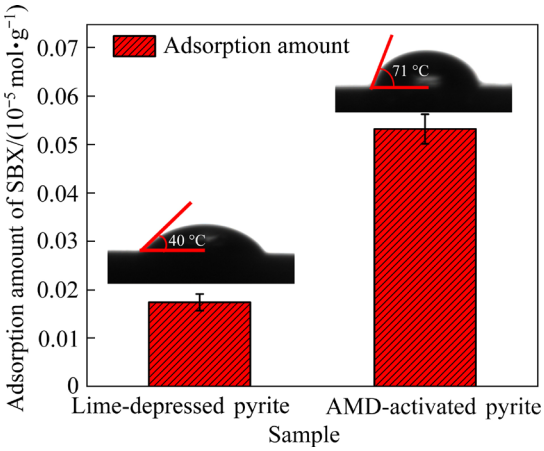

Fig. 5 Adsorption amount and contact angle of lime-depressed pyrite surface after interaction with SBX collector in the absence and presence of AMD

indicating that the introduction of AMD remarkably improved the hydrophobicity and floatability of pyrite once inhabited by lime. Also, previous studies [10,19,20,33] have indicated that Cu(I)-xanthate species and dixanthogen formed in the presence of copper ions through the reduction of Cu(II) and the oxidation of surface sulfides, resulting in improved pyrite hydrophobicity. Thus, it could be inferred that the adsorption of copper ions introduced by AMD on the pyrite surface benefited the formation of Cu(I)-xanthate species and dixanthogen, and contributed to the activation of pyrite flotation.

3.2.2 Raman spectra

The Raman spectra of lime-depressed pyrite samples before and after AMD activation are shown in Fig. 6. Meanwhile, the Raman spectrum of chalcopyrite was analyzed as a reference to investigate the effect of AMD on the surface sulfides of pyrite. For the chalcopyrite sample, the characteristic peaks at 285 and 462 cm^{-1} were assigned to the vibration of the Cu—S and Fe—S bonds [34]. For the pyrite−CaO sample, three characteristic peaks of lime-depressed pyrite were located at 334, 367, and 415 cm^{-1}, respectively. The peak at 334 cm^{-1} was attributed to the deformation vibration of Fe—$(S_2)^{2-}$, whereas the peaks at 367 and 415 cm^{-1} corresponded to the stretching vibration of Fe—$(S_2)^{2-}$ and S—S, respectively [35−37]. After AMD treatment, new peaks at 206, 262, and 477 cm^{-1} were observed on the lime-depressed pyrite surface. The peak located at 206 cm^{-1} was assigned to S^0, whereas the peaks located at 262 and

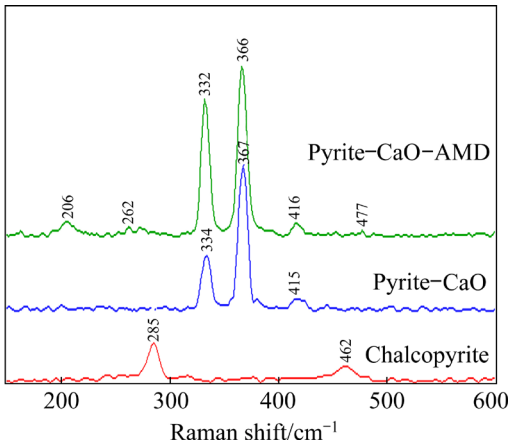

Fig. 6 Raman spectra of chalcopyrite and lime-depressed pyrite before (pyrite−CaO) and after (pyrite−CaO−AMD) AMD activation

477 cm^{-1} were assigned to the Cu—S bond, which well agreed with previous results [34,38,39], and the Raman spectra of chalcopyrite, respectively. These results demonstrated that AMD treatment promoted the formation of new hydrophobic species (S^0 hydrophobic entity and copper sulfides similar to chalcopyrite) on the pyrite surface. This activity may play a vital role in the AMD activation on the flotation of lime-inhibited pyrite.

3.2.3 Broad scan analysis results of XPS

Figure 7 exhibits the XPS survey spectra and elemental quantification of lime-depressed pyrite surfaces before and after AMD activation. As indicated in Fig. 7, the O and Ca contents on the pyrite−CaO surface were 38.94 at.% and 1.00 at.%, respectively, illustrating that pyrite experienced serious oxidation in the high-alkali lime system (pH 11.3), promoting the formation of hydrophilic calcium and iron species on the surface of minerals. When the lime-depressed pyrite was activated by AMD, the Ca and Fe contents were decreased to 0.052 at.% and 3.04 at.%, respectively. These results indicated that AMD can effectively remove the hydrophilic calcium and iron species, thus improving the activity of the pyrite once restrained by lime. It is noteworthy that significant increase in oxygen content (49.47 at.%) was observed after AMD treatment. This phenomenon may be attributed to the adsorption of SO_4^{2-} stemming from AMD. Moreover, the XPS spectrum of pyrite−CaO−AMD surface had a new peak at 932.6 eV, which was identified as a Cu 2p signal based on reported data [31]. The copper content was approximately 1.05 at.%. This result confirmed that the Cu^{2+} originating from AMD was adsorbed on the pyrite surface and facilitated the formation of hydrophobic copper sulfides. The broad scan analysis results of XPS were consistent with the observations on the flotation experiments, as well as the variation in Cu^{2+} content in flotation pulp.

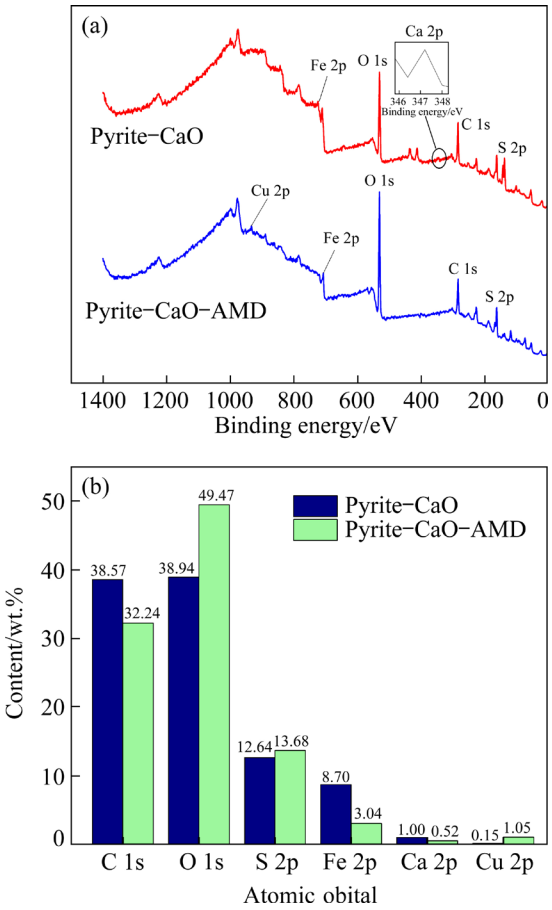

Fig. 7 XPS survey spectra (a) and element contents (b) of lime-depressed pyrite before and after AMD activation

(1) S 2p and Fe 2p spectra

Figure 8 presents the S 2p and Fe 2p XPS spectra recorded on the surface of lime-depressed pyrite before and after AMD activation. As observed from S 2p spectra of the lime-depressed pyrite, the characteristic peaks were located at 161.62, 162.58, and 163.79 eV, corresponding to monosulfide (S^{2-}), disulfide (S_2^{2-}), and polysulfide (S_n^{2-}) species, respectively [38,40,41]. The peak located at 168.48 eV was assigned to SO_4^{2-} [40]. The results indicated that the surficial sulfur of pyrite underwent oxidation in the high-alkali lime system (pH 11.3). When AMD was added, the SO_4^{2-} content on the pyrite surface significantly increased from 19.97% to 26.17%. It is possible that the SO_4^{2-}

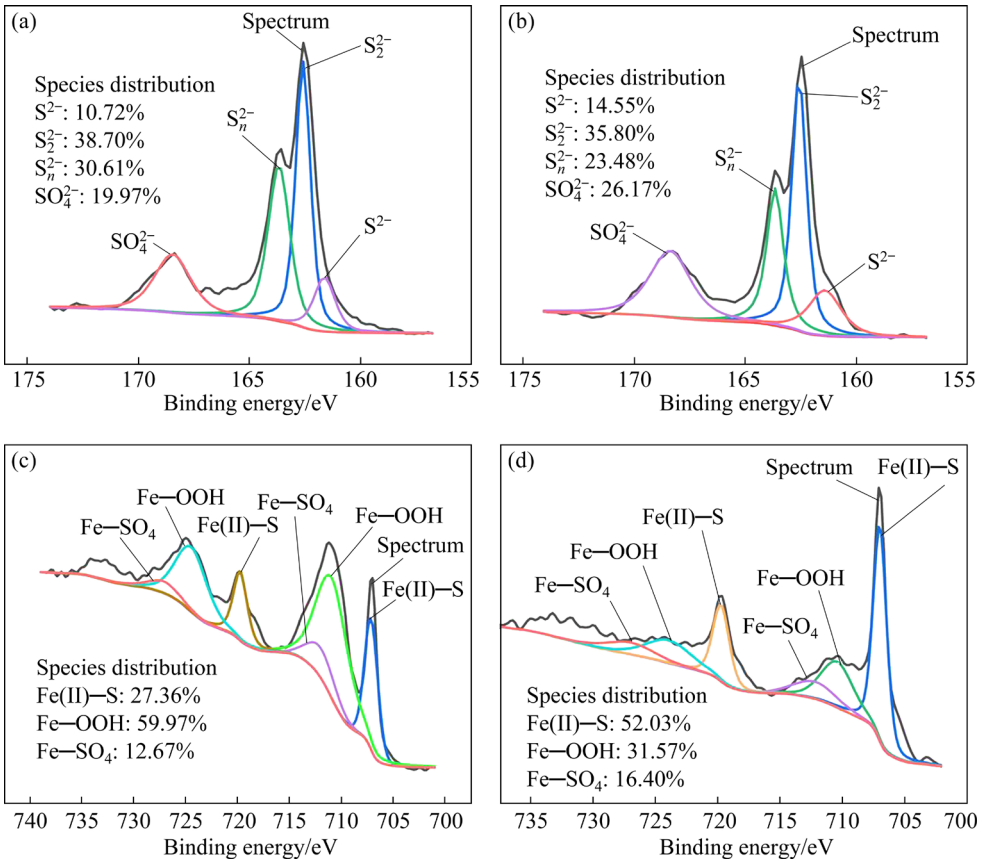

Fig. 8 S 2p (a, b) and Fe 2p (c, d) XPS spectra of lime-depressed pyrite surface before (a, c) and after (b, d) AMD activation

originating from AMD may be adsorbed on the pyrite surface, and the oxidation of surficial sulfur also contributed to the increase of SO_4^{2-}. The proportion of S^{2-} increased from 10.72% to 14.55%, whereas those of S_2^{2-} and S_n^{2-} decreased by 2.90% and 7.13%, respectively. This finding was due to the oxidation of pyrite and the adsorption of copper ions during AMD activation [33]. Notably, the S_2^{2-} and S_n^{2-} species played a vital role in pyrite flotation. However, adding AMD failed to reinforce these hydrophobic sulfur species on the pyrite surface. Thus, it was inferred that AMD activation on the flotation of lime-depressed pyrite in this study was mainly attributed to the removal of the hydrophilic calcium and iron species and the formation of new hydrophobic copper sulfides.

In the Fe 2p spectra of the lime-depressed pyrite sample, Fe 2p was fitted with Fe(II)—S (707.12 eV), Fe—OOH (710.89 eV) and Fe—SO_4 (711.97 eV), respectively [38,42,43]. The presence of substantial amount of Fe—OOH (59.97%) and Fe—SO_4 (12.67%) confirmed that the lime-depressed pyrite surfaces were wrapped by hydrophilic calcium and iron species, which were responsible for pyrite inhibition. After AMD activation, the proportion of Fe—S remarkably increased by 24.67%, and the Fe—OOH proportion decreased sharply from 59.97% to 31.57%. Meanwhile, the Fe—SO_4 proportion increased by 3.73%. Thus, it can be concluded that the introduction of AMD can effectively eliminate the hydrophilic iron species owing to the interaction between the Fe—OOH species and H^+, which was beneficial to restoring the activity of lime-inhibited pyrite. Notably, the adsorption of SO_4^{2-} stemming from AMD can increase the hydrophilicity of pyrite surfaces to some degree.

(2) Ca 2p and Cu 2p spectra

Figure 9 illustrates the XPS spectra of Ca 2p and Cu 2p recorded on the surface of lime-depressed pyrite before and after AMD activation. As indicated in the Ca 2p spectra before AMD activation (Fig. 9(a)), the characteristic peaks were located at 346.54 and 347.56 eV, corresponding to $CaSO_4$ and Ca—O/OH species, respectively [14,44]. The proportions of $CaSO_4$ and Ca—O/OH were

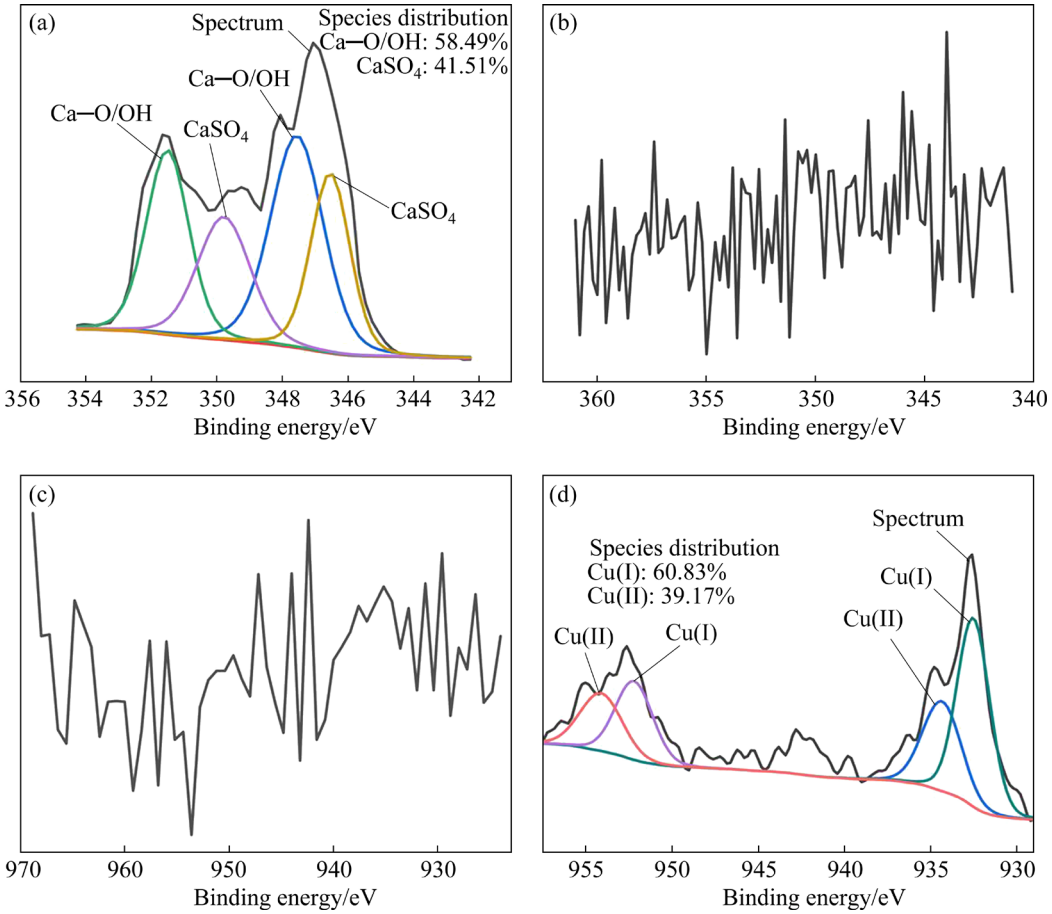

Fig. 9 Ca 2p (a, b) and Cu 2p (c, d) XPS spectra of lime-depressed pyrite surface before (a, c) and after (b, d) AMD activation

58.49% and 41.51%, respectively, confirming that the pyrite surfaces after the lime treatment were wrapped by hydrophilic calcium species and experienced severe inhibition. The Ca 2p peaks disappeared and failed to be identified in the XPS-extended energy spectrum analysis after AMD activation (Fig. 9(b)). These results indicated that the hydrophilic calcium overlays were effectively removed from the pyrite surface with the addition of AMD, resulting in the improved pyrite floatability.

There was no Cu 2p peak observed before AMD activation, which was not identified in the XPS-extended energy spectrum analysis results (Fig. 9(c)). It can be seen from the Cu 2p spectrum acquired in the high resolution XPS survey on lime-depressed pyrite surfaces after AMD activation (Fig. 9(d)). The main peak at 932.53 eV represented the Cu(I) formation on the pyrite surface, whereas the peak at 934.36 eV was assigned as Cu(II) [31,45]. It is well accepted that the Cu(I)−S species formed by the copper ion activation plays an important role in the pyrite flotation at mildly acidic pH [19]. EJTEMAEI and NGUYEN [38] proposed that a $CuFeS_2$-type layer may be formed in the presence of copper ions, and Cu(I)−S species dominate the sulfide mineral on pyrite surfaces. OERTZEN et al [46] suggested that $Cu_{3x}FeS_{2-x}$ surface species are generated after the complex redox reaction between Cu(II) and surficial sulfur during copper adsorption process, thereby contributing to the activation products for the pyrite flotation. The reaction can be represented by

$$FeS_2+3xCu^{2+}+4xH_2O= Cu_{3x}FeS_{2-x}+xSO_4^{2-}+8H^+ \quad (2)$$

The Cu $2p_{3/2}$ peaks of species such as $CuFeS_2$ may also appear at 932.30 eV [47,48]. The detection of Cu(I) in this study coincides with that previously reported for Cu-activated pyrite. Based on the basis of XPS and Raman spectroscopy analysis, it can be concluded that new hydrophobic

copper sulfide species formed on the pyrite surface, which were similar to chalcopyrite during AMD activation. Meanwhile, the oxidation of Cu(I)−S surface species under alkaline conditions was unavoidable, and the adsorption of the hydroxide precipitation onto inevitably occurred, thereby generating Cu(II) oxide/hydroxides overlays covering the pyrite surface. This accounts for the detection of Cu(II). Given these results, the activation of AMD on the lime-depressed pyrite may be attributed to the formation of Cu-activation products (new hydrophobic copper sulfide species), as well as the removal of hydrophilic calcium and iron species on the pyrite surfaces, thereby facilitating the adsorption of the collector.

Based on the aforementioned results and discussion, a schematic representing the AMD activation for the lime-depressed pyrite flotation was constructed and shown in Fig. 10. A substantial amount of hydrophilic calcium and iron species were wrapped on the pyrite surface depressed by lime. When AMD was added, the H^+ and SO_4^{2-} promoted the desorption of hydrophilic calcium and iron species from the pyrite surface mainly via acid−base neutralization and precipitation, resulting in the formation of $CaSO_{4(s)}$ and $Fe(OH)_{3(s)}$ in the pulp. Meanwhile, copper ions originating from AMD were adsorbed on the pyrite surface and promoted the formation of new hydrophobic species (S^0 hydrophobic entity and copper sulfides). With further addition of SBX collector, dixanthogen and Cu(I)-xanthate species formed and interacted with the pyrite surface. As a result, the lime-depressed pyrite floatability was improved considerably. The findings of the present theoretical research well explained the flotation behavior of lime-depressed pyrite from the tailings of Cu differential flotation with AMD activation. The application of AMD in pyrite activation can be expected to solve the negative impacts of AMD on the environment at its source and increase the beneficiation effects. Therefore, this study can serve as an important theoretical basis and technical support for the cleaner production of copper sulfide ore.

4 Conclusions

(1) Flotation test results showed that AMD can effectively activate pyrite flotation with SBX collector from the tailings of Cu differential flotation with high-alkali lime, and a high-quality sulfur concentrate with 51.08% S grade and 82.95% S recovery was obtained.

(2) AMD facilitated the desorption of Ca^{2+} located on the lime-depressed pyrite surface and increased the hydrophobicity of the pyrite. Meanwhile, the actual Cu^{2+} concentrations in the pulp were all below 0.02 mg/L, and Cu^{2+} originating from the AMD can be adsorbed onto the pyrite surface completely. Adsorption measurements and contact angle analysis confirmed that adding AMD improved the adsorption amount of SBX collector from 0.018×10^{-5} to 0.053×10^{-5} mol/g and increased the contact angle by 31°. Results of Raman spectroscopy and XPS analysis indicated that AMD treatment promoted the formation of new hydrophobic species (S^0 hydrophobic entity, and copper sulfides similar to chalcopyrite) on the pyrite surface.

(3) The activation of AMD on lime-depressed pyrite may be attributed to the formation of new hydrophobic species, as well as the removal of hydrophilic calcium and iron species on the pyrite surfaces, which reinforced the adsorption of the collector. Therefore, the findings of the present research well explained the flotation behavior and mechanism of lime-depressed pyrite with AMD as a

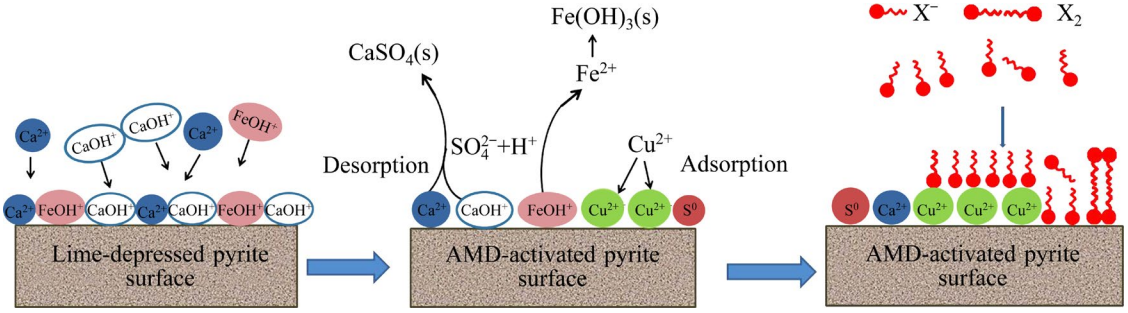

Fig. 10 Schematic representation of AMD activation for lime-depressed pyrite flotation

natural activator, providing an important theoretical basis and technical support for the cleaner production of copper sulfide ore.

CRediT authorship contribution statement

Jia-qiao YUAN: Conceptualization, Data curation, Writing − Review & editing; **Zhan DING:** Investigation, Data curation; **Yun-xiao BI:** Conceptualization, Methodology; **Jie LI:** Visualization, Investigation; **Shu-ming WEN:** Methodology, Supervision; **Shao-jun BAI:** Conceptualization, Methodology, Writing − Review & editing.

Declaration of competing interest

The authors declare that they have no known competing financial interests or personal relationships that could have appeared to influence the work reported in this paper.

Acknowledgments

This work was financially supported from the National Natural Science Foundation of China (No. 52164021), and the Natural Science Foundation of Yunnan Province, China (No. 2019FB078).

References

[1] HUANG Zi-jie, WANG Jian-jun, SUN Wei, HU Yue-hua, CAO Jian, GAO Zhi-yong. Selective flotation of chalcopyrite from pyrite using diphosphonic acid as collector [J]. Minerals Engineering, 2019, 140: 105890.

[2] KHOSO S A, GAO Zhi-yong, SUN Wei. Recovery of high-grade copper concentrate from sulfur-rich porphyry ore using tricarboxystarch micromolecule as pyrite depressant [J]. Minerals Engineering, 2021, 168: 106916.

[3] MU Yu-fan, PENG Yong-jun, LAUTEN R A. The depression of copper-activated pyrite in flotation by biopolymers with different compositions [J]. Minerals Engineering, 2016, 96/97: 113−122.

[4] LÜ Cui-cui, WANG Yong-liang, QIAN Peng, LIU Ya, FU Guo-yan, DING Jian, YE Shu-feng, CHEN Yuan-fa. Separation of chalcopyrite and pyrite from a copper tailing by ammonium humate [J]. Chinese Journal of Chemical Engineering, 2018, 26: 1814−1821.

[5] BU Xian-zhong, FENG Yuan-yuan, XUE Ji-wei, YANG Lu, ZHANG Chong-hui. Effective recovery of chalcopyrite at low temperatures using modified ester collector [J]. Transactions of Nonferrous Metals Society of China, 2022, 32: 296−306.

[6] HAN Guang, WEN Shu-ming, WANG Han, FENG Qi-cheng, BAI Xu. Pyrogallic acid as depressant for flotation separation of pyrite from chalcopyrite under low-alkalinity conditions [J]. Separation and Purification Technology, 2021, 267: 118670.

[7] CAO Fei, SUN De-si, QIU Xian-hui, ZHOU De-zhi, ZHANG Xing-rong, SUN Chuan-yao. Synthesis of novel thionocarbamate for copper−sulfur flotation separation and its adsorption mechanism [J]. Transactions of Nonferrous Metals Society of China, 2022, 32: 2709−2718.

[8] LI Yu-qiong, CHEN Jian-hua, KANG Duan, GUO Jin. Depression of pyrite in alkaline medium and its subsequent activation by copper [J]. Minerals Engineering, 2012, 26: 64−69.

[9] ZANIN M, LAMBERT H, DU PLESSIS C A. Lime use and functionality in sulphide mineral flotation: A review [J]. Minerals Engineering, 2019, 143: 105922.

[10] CHANDRA A P, GERSON A R. A review of the fundamental studies of the copper activation mechanisms for selective flotation of the sulfide minerals, sphalerite and pyrite [J]. Advances in Colloid and Interface Science, 2009, 145: 97−110.

[11] YIN Wan-zhong, YANG Bin, FU Ya-feng, CHU Fu-dong, YAO Jin, CAO Shao-hang, ZHU Zhang-lei. Effect of calcium hypochlorite on flotation separation of covellite and pyrite [J]. Powder Technology, 2019, 343: 578−585.

[12] CRUNDWELL F K. The impact of light on understanding the mechanism of dissolution and leaching of sphalerite (ZnS), pyrite (FeS_2) and chalcopyrite ($CuFeS_2$) [J]. Minerals Engineering, 2021, 161: 106728.

[13] MAFRA C, BOUZAHZAH H, STAMENOV L, GAYDARDZHIEV S. Insights on the effect of pyrite liberation degree upon the acid mine drainage potential of sulfide flotation tailings [J]. Applied Geochemistry, 2020, 123: 104774.

[14] HU Yue-hua, ZHANG Shun-li, QIU Guan-zhou, MILLER J D. Surface chemistry of activation of lime-depressed pyrite in flotation [J]. Transactions of Nonferrous Metals Society of China, 2000, 10: 798−803.

[15] HUANG Hong-jun, HU Yue-hua, SUN Wei. Activation flotation and mechanism of lime-depressed pyrite with oxalic acid [J]. International Journal of Mining Science and Technology, 2012, 22: 63−67.

[16] TANG Xue-kun, CHEN Yan-fei. Using oxalic acid to eliminate the slime coatings of serpentine in pyrite flotation [J]. Minerals Engineering, 2020, 149: 106228.

[17] LIU Jie, LI Er-lei, JIANG Kai, LI Yan-jun, HAN Yue-xin. Effect of acidic activators on the flotation of oxidized pyrrhotite [J]. Minerals Engineering, 2018, 120: 75−79.

[18] DENG Zheng-bin, CHENG Wan-li, TANG Yun, TONG Xiong, LIU Zhi-hong. Adsorption mechanism of copper xanthate on pyrite surfaces [J]. Physicochemical Problems of Mineral Processing, 2021, 57: 46−60.

[19] LEPPINEN J O. FTIR and flotation investigation of the adsorption of ethyl xanthate on activated and non-activated sulfide minerals [J]. International Journal of Mineral Processing, 1990, 30: 245−263.

[20] SHEN W Z, FORNASIERO D, RALSTON J. Flotation of sphalerite and pyrite in the presence of sodium sulfite [J]. International Journal of Mineral Processing, 2001, 63:

17−28.

[21] JEONG J, KIM M S, KIM B S, KIM S K, KIM W B, LEE J C. Recovery of H2SO4 from waste acid solution by a diffusion dialysis method [J]. Journal of Hazardous Materials, 2005, 124: 230−235.

[22] JOHNSON D B, HALLBERG K B. Acid mine drainage remediation options: A review [J]. The Science of the Total Environment, 2005, 338: 3−14.

[23] ABROSIMOVA N, GASKOVA O, LOSHKAREVA A, EDELEV A, BORTNIKOVA S. Assessment of the acid mine drainage potential of waste rocks at the Ak-Sug porphyry Cu−Mo deposit [J]. Journal of Geochemical Exploration, 2015, 157: 1−14.

[24] HAN Y S, YOUM S J, OH C, CHO Y C, AHN J S. Geochemical and eco-toxicological characteristics of stream water and its sediments affected by acid mine drainage [J]. Catena, 2017, 148: 52−59.

[25] YUAN Jia-qiao, DING Zhan, BI Yun-xiao, LI Jie, WEN Shu-ming, BAI Shao-jun. Resource utilization of acid mine drainage (AMD): A review [J]. Water, 2022, 14: 2385.

[26] IGARASHI T, HERRERA P S, UCHIYAMA H, MIYAMAE H, IYATOMI N, HASHIMOTO K, TABELIN C B. The two-step neutralization ferrite-formation process for sustainable acid mine drainage treatment: Removal of copper, zinc and arsenic, and the influence of coexisting ions on ferritization [J]. The Science of the Total Environment, 2020, 715: 136877.

[27] KAUR G, COUPERTHWAITE S J, MILLAR G J. Alternative neutralisation materials for acid mine drainage treatment [J]. Journal of Water Process Engineering, 2018, 22: 46−58.

[28] NARIYAN E, WOLKERSDORFER C, SILLANPAA M. Sulfate removal from acid mine water from the deepest active European mine by precipitation and various electro-coagulation configurations [J]. Journal of Environmental Management, 2018, 227: 162−171.

[29] PAT-ESPADAS A, LOREDO PORTALES R, AMABILIS-SOSA L, GÓMEZ G, VIDAL G. Review of constructed wetlands for acid mine drainage treatment [J]. Water, 2018, 10: 1685.

[30] TAN L C, PAPIRIO S, LUONGO V, NANCHARAIAH Y V, CENNAMO P, ESPOSITO G, HULLEBUSCH E D, LENS P N L. Comparative performance of anaerobic attached biofilm and granular sludge reactors for the treatment of model mine drainage wastewater containing selenate, sulfate and nickel [J]. Chemical Engineering Journal, 2018, 345: 545−555.

[31] BAI Shao-jun, BI Yun-xiao, LI Jie, YU Pan, DING Zhan, LV Chao, WEN Shu-ming. Innovative utilization of acid mine drainage (AMD): A promising activator for pyrite flotation once depressed in a high alkali solution (HAS)–Gearing towards a cleaner production concept of copper sulfide ore [J]. Minerals Engineering, 2021, 170: 106997.

[32] YANG Xu, LI Yu-biao, FAN Rong, DUAN Wan-qing, HUANG Ling-yun, XIAO Qing. Separation mechanism of chalcopyrite and pyrite due to H_2O_2 treatment in low-alkaline seawater flotation system [J]. Minerals Engineering, 2022, 176: 107356.

[33] CHANDRA A P, PUSKAR L, SIMPSON D J, GERSON A R. Copper and xanthate adsorption onto pyrite surfaces: Implications for mineral separation through flotation [J]. International Journal of Mineral Processing, 2012, 114/115/116/117: 16−26.

[34] URBANO G, LÁZARO I, RODRÍGUEZ I, REYES J L, LARIOS R, CRUZ R. Electrochemical and spectroscopic study of interfacial interactions between chalcopyrite and typical flotation process reagents [J]. International Journal of Minerals, Metallurgy, and Materials, 2016, 23: 127−136.

[35] WANG Chong-qing, SUN Rui-rui, HUANG Rong, CAO Yi-jun. A novel strategy for enhancing heterogeneous Fenton degradation of dye wastewater using natural pyrite: Kinetics and mechanism [J]. Chemosphere, 2021, 272: 129883.

[36] XIA Jin-lan, YANG Yi, HE Huan, ZHAO Xiao-juan, LIANG Chang-li, ZHENG Lei, MA Chen-yan, ZHAO Yi-dong, NIE Zhen-yuan, QIU Guan-zhou. Surface analysis of sulfur speciation on pyrite bioleached by extreme thermophile *Acidianus manzaensis* using Raman and XANES spectroscopy [J]. Hydrometallurgy, 2010, 100: 129−135.

[37] YUAN Xue-yin, ZHENG Hai-fei. In situ Raman spectroscopic studies of FeS_2 pyrite up to 675 K and 2100 MPa using a hydrothermal diamond anvil cell [J]. Mineralogical Magazine, 2015, 79: 1−10.

[38] EJTEMAEI M, NGUYEN A V. Characterisation of sphalerite and pyrite surfaces activated by copper sulphate [J]. Minerals Engineering, 2017, 100: 223−232.

[39] PARKER G K, WOODS R, HOPE G A. Raman investigation of chalcopyrite oxidation [J]. Colloids and Surfaces A: Physicochemical and Engineering Aspects, 2008, 318: 160−168.

[40] CAI Yuan-feng, PAN Yu-guan, XUE Ji-yue, SUN Qing-feng, SU Gui-zhen, LI Xiang. Comparative XPS study between experimentally and naturally weathered pyrites [J]. Applied Surface Science, 2009, 255: 8750−8760.

[41] HAN Guang, WEN Shu-ming, WANG Han, FENG Qi-cheng. Enhanced sulfidization flotation of cuprite by surface modification with hydrogen peroxide [J]. Transactions of Nonferrous Metals Society of China, 2021, 31: 3564−3578.

[42] WANG Chang-tao, LIU Run-qing, KHOSO S A, LU Hong-yu, SUN Wei, NI Zhang-yuan, LYU Fei. Combined inhibitory effect of calcium hypochlorite and dextrin on flotation behavior of pyrite and galena sulphides [J]. Minerals Engineering, 2020, 150: 106274.

[43] ZHANG Xiao-long, QIN Yong-hong, HAN Yue-xin, LI Yan-jun, GAO Peng, LI Guo-feng, WANG Shao-xing. A potential ceramic ball grinding medium for optimizing flotation separation of chalcopyrite and pyrite [J]. Powder Technology, 2021, 392: 167−178.

[44] BAI Shao-jun, YU Pan, LI Chun-long, WEN Shu-ming, DING Zhan. Depression of pyrite in a low-alkaline medium with added calcium hypochlorite: Experiment, visual MINTEQ models, XPS, and ToF–SIMS studies [J]. Minerals Engineering, 2019, 141: 105853.

[45] BIESINGER M C. Advanced analysis of copper X-ray

photoelectron spectra [J]. Surface and Interface Analysis, 2017, 49: 1325−1334.

[46] von OERTZEN G U, SKINNER W M, NESBITT H W, PRATT A R, BUCKLEY A N. Cu adsorption on pyrite (100): Ab initio and spectroscopic studies [J]. Surface Science, 2007, 601: 5794−5799.

[47] GHAHREMANINEZHAD A, DIXON D G, ASSELIN E. Electrochemical and XPS analysis of chalcopyrite ($CuFeS_2$) dissolution in sulfuric acid solution [J]. Electrochimica Acta, 2013, 87: 97−112.

[48] YANG Bing-qiao, YAN Hai, ZENG Meng-yuan, HUANG Peng-liang, JIA Fei-fei, TENG Ai-ping. A novel copper depressant for selective flotation of chalcopyrite and molybdenite [J]. Minerals Engineering, 2020, 151: 106309.

酸性矿山废水对硫化铜矿中石灰抑制黄铁矿浮选的活化机理

袁加巧[1]，丁 湛[1]，毕云霄[1]，李 颉[1]，文书明[1,2,3]，柏少军[1,2,3]

1. 昆明理工大学 国土资源工程学院，昆明 650093；
2. 昆明理工大学 复杂有色金属资源清洁利用国家重点实验室，昆明 650093；
3. 昆明理工大学 云南省战略金属矿产资源绿色分离与富集重点实验室，昆明 650093

摘 要：以酸性矿山废水(AMD)为天然活化剂，从铜优先浮选尾矿中回收被石灰抑制的黄铁矿。通过一系列实验室浮选试验和表面分析技术研究 AMD 对石灰抑制黄铁矿浮选的影响。浮选试验结果表明，以丁基黄药(SBX)为捕收剂，AMD 能够有效地活化黄铁矿浮选，并获得高品质的硫精矿。矿浆离子浓度分析结果表明，AMD 促进了被抑制黄铁矿表面 Ca^{2+}的解吸和 Cu^{2+}的吸附。吸附测量和接触角分析结果表明，加入 AMD 后，SBX 在黄铁矿表面的吸附量增加，其接触角增加了 31°。拉曼光谱和 X 射线光电子能谱分析结果表明，AMD 的添加促进了疏水性物种(S^0 疏水体和硫化铜物种)的形成，并去除了黄铁矿表面的亲水性钙和铁物种，从而加强了捕收剂在黄铁矿表面的吸附作用。本研究为硫化铜矿的清洁生产提供了重要的理论依据和技术支持。

关键词：硫化铜矿；酸性矿山废水；石灰抑制黄铁矿；浮选；天然活化剂；活化机理

(Edited by Wei-ping CHEN)